Journal of Power Sources 184 (2008) 414–419

Contents lists available at ScienceDirect

Journal of Power Sources

journal homepage: www.elsevier.com/locate/jpowsour

Structural and electrochemical characterization of $xLi[Li_{1/3}Mn_{2/3}]O_2\cdot(1-x)Li[Ni_{1/3}Mn_{1/3}Co_{1/3}]O_2$ $(0\le x\le 0.9)$ as cathode materials for lithium ion batteries

Xiao-Jian Guo, Yi-Xiao Li, Min Zheng, Jian-Ming Zheng, Jie Li, Zheng-Liang Gong, Yong Yang*

State Key Laboratory for Physical Chemistry of Solid Surfaces, Department of Chemistry, Xiamen University, Xiamen 361005, PR China

ARTICLE INFO

Article history:
Received 4 January 2008
Received in revised form 1 April 2008
Accepted 2 April 2008
Available online 12 April 2008

Keywords:
$xLi[Li_{1/3}Mn_{2/3}]O_2\cdot(1-x)Li[Ni_{1/3}Mn_{1/3}Co_{1/3}]O_2$
Cathode
Lithium ion batteries

ABSTRACT

A series of cathode materials with molecular notation of $xLi[Li_{1/3}Mn_{2/3}]O_2\cdot(1-x)Li[Ni_{1/3}Mn_{1/3}Co_{1/3}]O_2$ $(0\le x\le 0.9)$ were synthesized by combination of co-precipitation and solid state calcination method. The prepared materials were characterized by X-ray diffraction (XRD) and X-ray photoelectron spectroscopy (XPS) techniques, and their electrochemical performances were investigated. The results showed that sample $0.6Li[Li_{1/3}Mn_{2/3}]O_2\cdot 0.4Li[Ni_{1/3}Mn_{1/3}Co_{1/3}]O_2$ ($x=0.6$) delivers the highest capacity and shows good capacity-retention, which delivers a capacity ~250 mAh g^{-1} between 2.0 and 4.8 V at 18 mA g^{-1}.

1. Introduction

$Li[Ni_{1/3}Mn_{1/3}Co_{1/3}]O_2$ and relative compounds are a promising class of cathode materials [1–6] because of its high specific capacity, low cost, environmental-friendly and mild character with electrolyte when charged to higher potential than that of charged $LiNiO_2$ and $LiCoO_2$ [7]. Li_2MnO_3 adopts a layered structure with Li:Mn = 1:2 in transitional metal layer [8]. In addition, $xLi[Li_{1/3}Mn_{2/3}]O_2\cdot(1-x)LiMO_2$ (M = Mn, Ni) has also been investigated by many groups in recent years [9–11], the $Li[Li_{1/3}Mn_{2/3}]O_2$ component can provide additional stability to the layered $Li[Ni_{1/3}Mn_{1/3}Co_{1/3}]O_2$ electrode thus improve the performance of the layered intercalation material [11]. $xLi[Li_{1/3}Mn_{2/3}]O_2\cdot(1-x)LiMO_2$ (M = Mn, Ni) materials delivered high specific capacity but showed poor electronic conductivity. Doping cobalt is an effective way to enhance the electronic conductivity of the materials [12]. The mechanism of anomalous capacity when charging Li_2MnO_3 to 4.8 V is not well-defined up to now. Bruce and coworkers [13] have reported that H^+ transfer dominated this procedure when charged and discharged at 55 °C. At 30 °C initial Li^+ removal was accompanied by oxygen loss (effective removal of Li_2O) but further Li^+ removal involved the same proton exchange mechanism as observed at 55 °C. This work was proved by experiment of TGA-MS. Thackeray's group [14] reported that when $xLi_2MnO_3\cdot(1-x)LiMn_{0.5}Ni_{0.5}O_2$ was charged to 5 V, the first step in the charging curves predominantly corresponded to Li^+ extraction from the host with oxidation of Ni^{2+} to Ni^{4+}, and the second step corresponded to the electrochemical removal of Li_2O from the structure. Dahn's group also reported that the second extraction of Li^+ from the electrode $Li[Ni_xLi_{1/3-2x/3}Mn_{2/3-x/3}]O_2$ was due to the simultaneous extraction of Li^+ and O^{2-} from the host structure. They approved this by doing ex situ XRD of fully charged electrode and Rietveld refinement to find the O^{2-} occupation of material [10,15]. They assumed that when fully discharged, all Li^+ filled the Li^+ layer for samples with $x\ge 1/3$ [15].

In this paper, a series of cathode materials with molecular notation of $xLi[Li_{1/3}Mn_{2/3}]O_2\cdot(1-x)Li[Ni_{1/3}Mn_{1/3}Co_{1/3}]O_2$ $(0\le x\le 0.9)$ were synthesized by combination of co-precipitation and solid state calcination method. $xLi[Li_{1/3}Mn_{2/3}]O_2\cdot(1-x)Li[Ni_{1/3}Mn_{1/3}Co_{1/3}]O_2$ samples prepared by this method delivers a high capacity of 250 mAh g^{-1} and shows good cyclic performance at $x=0.6$.

2. Experimental

2.1. Powder preparation

The materials with stoichiometry of $xLi[Li_{1/3}Mn_{2/3}]O_2\cdot(1-x)$-$Li[Ni_{1/3}Mn_{1/3}Co_{1/3}]O_2$ $(0\le x\le 0.9)$ were prepared by combination of co-precipitation and solid state calcination method. Acetates of

* Corresponding author. Tel.: +86 592 2185753; fax: +86 592 2185753.
E-mail address: yyang@xmu.edu.cn (Y. Yang).

0378-7753/$ – see front matter © 2008 Elsevier B.V. All rights reserved.
doi:10.1016/j.jpowsour.2008.04.013

nickel, manganese and cobalt were dissolved in distilled water with stoichiometric ratio of $(1-x)$:$(1+x)$:$(1-x)$, after stirring for 4 h, the prepared solution was dropped slowly to constantly stirred LiOH solution (1.25 M). The precipitate was washed three times with distilled water and dried in air at 120 °C for 20 h. Stoichiometric amount of LiOH and dried precipitate powder were mixed well by ball milling at 500 rpm for 7 h with petroleum ether as solvent. The powder mixture was pressed into pellets, packed in a ceramic boat, and calcined in air at 480 °C for 10 h. Then, the mixture was heated at 900 °C for another 3 h in quartz tube oven. After that, it was quenched to room temperature. All of the chemicals were AR grade.

2.2. Structural characterization

Crystal characterizations of the materials were performed with a Panalytical X'pert diffractometer (PANalytical, Netherlands) using Cu Kα radiation operated at 40 kV and 30 mA. X-ray photoelectron spectroscopy (XPS) of these samples were obtained using Quantum 2000 spectrometer (Physical Electronics, USA) with monochromatic Al Kα radiation ($h\nu$ = 1486.6 eV) to determine chemical valence state of transition elements. Binding energies were charge corrected using the C 1s peak (284.8 eV).

2.3. Electrochemical measurements

The electrochemistry characteristics of the prepared powders were tested using CR2025 coin cells as described in our previous publications [16]. The active materials, acetylene black and polyvinylidene fluoride (PVDF) were mixed in a weight ratio of 80:10:10 in *N*-methyl-2-pyrrolidene (NMP) and ball-milled for 3 h to make a slurry. The slurry was coated onto Al foils and pressed at 18 MPa after drying for 2 h at 120 °C in air. The cells were assembled in an argon filled glove box with the electrolytes of 1 M $LiPF_6$ dissolved in EC + DMC (1:1 volume ratio) and lithium as anode. Charge and discharge tests were all performed galvanostatically at 18 mA g^{-1} between 2.0 and 4.8 V by an Arbin BT-2043 battery testing system at 30 °C.

3. Results and discussion

3.1. Powder characteristics

The XRD patterns of the prepared powders are shown in Fig. 1. All the patterns can be indexed to a single phase of the α-$NaFeO_2$ type with space group *R*-3*m* except for the small peaks at 2θ = 20.85°, 21.79°, 24.31°, 28.81°, 58.9° which can be indexed to *C*2/*m* space group. Fig. 2 shows the lattice parameters of as-prepared materials calculated by the Rietveld method with General Structure Analysis Software (GSAS Los Alamos National Laboratory, USA). It shows that the *c*/*a* value increases with *x*, except for the sample with *x* = 0.9. However, *a*, *c* and the volume of the cell decrease with *x*. This may due to the larger electrostatic force between Mn^{4+} and oxygen anion layer.

Detailed high-resolution transmission electron microscopy (HRTEM), nuclear magnetic resonance (NMR), and computational studies, carried out previously, revealed that the structures of $x\mathrm{Li[Li_{1/3}Mn_{2/3}]O_2}\cdot(1-x)\mathrm{Li[Ni_{1/3}Mn_{1/3}Co_{1/3}]O_2}$ electrode materials are highly complex; they are characterized by short-range order of the cations extending to microphase separation [14,17,18]. As such, they can be described as having nanocomposite structures derived from a pseudo-binary $x\mathrm{Li[Li_{1/3}Mn_{2/3}]O_2}\cdot(1-x)\mathrm{Li[Ni_{1/3}Mn_{1/3}Co_{1/3}]O_2}$ system with Li_2MnO_3 and $\mathrm{Li[Ni_{1/3}Mn_{1/3}Co_{1/3}]O_2}$ end members [9]. The structure of Li_2MnO_3 is a rock-salt structure in which layers of Li^+ and

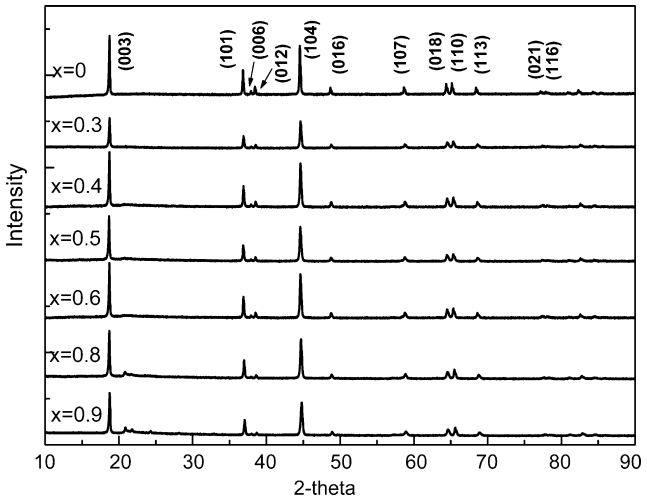

Fig. 1. XRD patterns of prepared powders $x\mathrm{Li[Li_{1/3}Mn_{2/3}]O_2}\cdot(1-x)\mathrm{Li[Ni_{1/3}Mn_{1/3}Co_{1/3}]O_2}$ $(0 \le x \le 0.9)$.

layers of Mn^{4+} and Li^+ (1:2) alternate between the close-packed oxygen layers [8]. As reported in the literature (0 1 8)/(1 1 0) peak splitting is considered as an evidence for the degree of ordering layered structure [19,20]. As is shown in Fig. 1, peaks (0 1 8) and (1 1 0) split larger with *x*, the difference of peaks (0 1 8) and (1 1 0) vs. *x* is shown in Fig. 3. This is consistent with the trends of *a*, *c*, *c*/*a* shown in Fig. 2. In Fig. 1, the peaks at 2θ = 20.85°, 21.79°, 24.31°, 28.81°, 58.9° are caused by the superlattice ordering of Li^+ and Mn^{4+} in transition metal layer [10]. It is reported [21] that Li^+ is surrounded by six Mn^{4+} ions with Li^+ in the center of the hexagon, as shown in Fig. 4(a). In addition, $\mathrm{Li[Ni_{1/3}Mn_{1/3}Co_{1/3}]O_2}$ has a rock-salt configuration too. There is a Li^+ layer and transition metal layer which consists of Ni^{2+}, Mn^{4+}, Co^{3+} with Ni^{2+} in the center of a hexagon and Mn^{4+}, Co^{3+} occupied the vertices of the hexagon alternately, as is shown in Fig. 4(b). For powder $x\mathrm{Li[Li_{1/3}Mn_{2/3}]O_2}\cdot(1-x)\mathrm{Li[Ni_{1/3}Mn_{1/3}Co_{1/3}]O_2}$ $(0 \le x \le 0.9)$, we assume these two figures alternate with the ratio of x:$(1-x)$ in transition metal layer.

The scanning electron micrographs of $x\mathrm{Li[Li_{1/3}Mn_{2/3}]O_2}\cdot(1-x)\mathrm{Li[Ni_{1/3}Mn_{1/3}Co_{1/3}]O_2}$ materials with *x* = 0.3 and *x* = 0.6 are shown

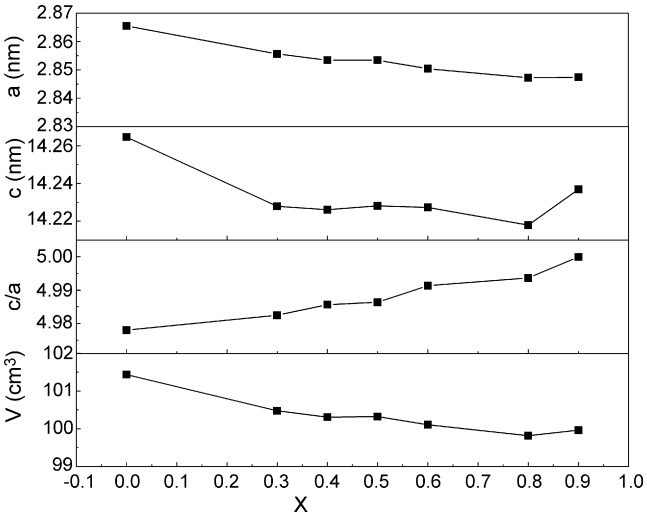

Fig. 2. Lattice parameters of prepared powders $x\mathrm{Li[Li_{1/3}Mn_{2/3}]O_2}\cdot(1-x)\mathrm{Li[Ni_{1/3}Mn_{1/3}Co_{1/3}]O_2}$ $(0 \le x \le 0.9)$ calculated by Rietveld analysis with GSAS software.

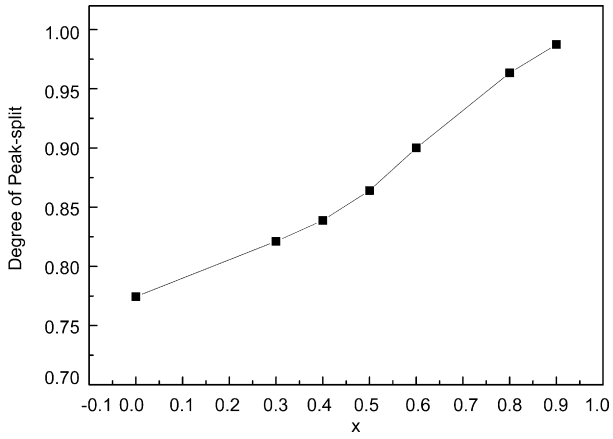

Fig. 3. Peak splitting of (0 1 8) and (1 1 0) vs. *x*.

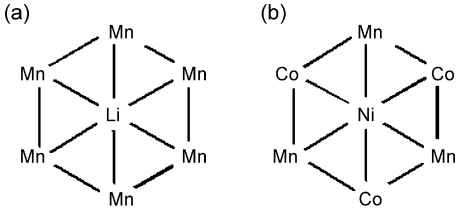

Fig. 4. The structure of transition metal layer of $Li[Li_{1/3}Mn_{2/3}]O_2$(a) and $Li[Ni_{1/3}Mn_{1/3}Co_{1/3}]O_2$ (b).

in Fig. 5. It shows that the particles of the two materials are homogeneously distributed with the particles sizes between 0.1 and 0.5 μm.

The Mn 2p, Ni 2p and Co 2p XPS spectra for $xLi[Li_{1/3}Mn_{2/3}]O_2\cdot(1-x)Li[Ni_{1/3}Mn_{1/3}Co_{1/3}]O_2$ $(0 \le x \le 0.9)$ materials are shown in Fig. 6. As is shown in Fig. 6, the binding energies of transition metal in different samples are almost the same. The binding energies of manganese $2p_{3/2}$ in $xLi[Li_{1/3}Mn_{2/3}]O_2\cdot(1-x)Li[Ni_{1/3}Mn_{1/3}Co_{1/3}]O_2$ $(0 \le x \le 0.9)$ are near 642.1 eV, BE of nickel $2p_{3/2}$ are 854.6 eV, BE of cobalt $2p_{3/2}$ are near 780.0 eV. We can assign the valence state of Mn, Ni, Co with +4, +2, +3.

3.2. Electrochemistry tests

Fig. 7 shows the initial charge–discharge curves for the $Li/xLi[Li_{1/3}Mn_{2/3}]O_2\cdot(1-x)Li[Ni_{1/3}Mn_{1/3}Co_{1/3}]O_2$ $(0 \le x \le 0.9)$ materials. It shows that layered $xLi[Li_{1/3}Mn_{2/3}]O_2\cdot(1-x)$-$Li[Ni_{1/3}Mn_{1/3}Co_{1/3}]O_2$ $(0 \le x \le 0.9)$ electrodes can provide remarkably high electrochemical capacities by activating the Li_2MnO_3 component above 4.4 V vs. Li/Li^+; the capacity and cycling stability is dependent on the value of *x*. As it is observed that prepared powder $xLi[Li_{1/3}Mn_{2/3}]O_2\cdot(1-x)Li[Ni_{1/3}Mn_{1/3}Co_{1/3}]O_2$ $(0 \le x \le 0.9)$ delivers high specific capacity, and the initial discharge capacities of electrodes with $x = 0.6$ and $x = 0.8$ are both higher than 200 mAh g^{-1}. A discharge capacity of 250 mAh g^{-1} is obtained for sample $0.6Li[Li_{1/3}Mn_{2/3}]O_2\cdot0.4Li[Ni_{1/3}Mn_{1/3}Co_{1/3}]O_2$ $(x = 0.6)$. On the initial charge to 4.8 V, the $0.6Li[Li_{1/3}Mn_{2/3}]O_2\cdot0.4Li[Ni_{1/3}Mn_{1/3}Co_{1/3}]O_2$ electrode delivers 306 mAh g^{-1}. And on the subsequent discharge to 2.0 V, 250 mAh g^{-1} is recovered from the electrode; this is value excellent consonant with the theoretical capacity from a fully delithiated $0.6[Mn_{2/3}]O_{4/3}\cdot0.4[Mn_{1/3}Co_{1/3}Ni_{1/3}]O_2$ electrode, namely 251 mAh g^{-1}, when the mass of the parent electrode is used for the calculation.

Fig. 8 shows the curves of differential capacity vs. voltage for discharging of prepared powders. For $xLi[Li_{1/3}Mn_{2/3}]O_2\cdot(1-x)Li[Ni_{1/3}Mn_{1/3}Co_{1/3}]O_2$ $(0 \le x \le 0.9)$, during the initial charging, the first peak can attributed to Li^+ extraction concomitant with the oxidation of Ni^{2+} and Co^{3+}, and the capacity after 4.4 V at which is accompanied with Li^+ and oxygen ions' extraction from the host, which is absent during the subsequent charge, is consistent with the irreversible removal of Li_2O from, electrochemical activation of, the Li_2MnO_3 component that occurs on the voltage plateau at 4.5–4.6 V [11,14]. The intensity of the peaks near 4.5 V, characteristic of irreversible lithium extraction from the transition metal layers, significantly increases with *x*, as expected, as shown in Fig. 8a. During the initial discharging, the first peak near 3.7 V is the reaction of reducing Ni^{4+} to Ni^{2+} and Co^{4+} to Co^{3+} with Li^+ reinserting to the host structure, the peak here shifts to lower potential and the intensity decreases with *x*. This is consistent with the lower content of nickel and

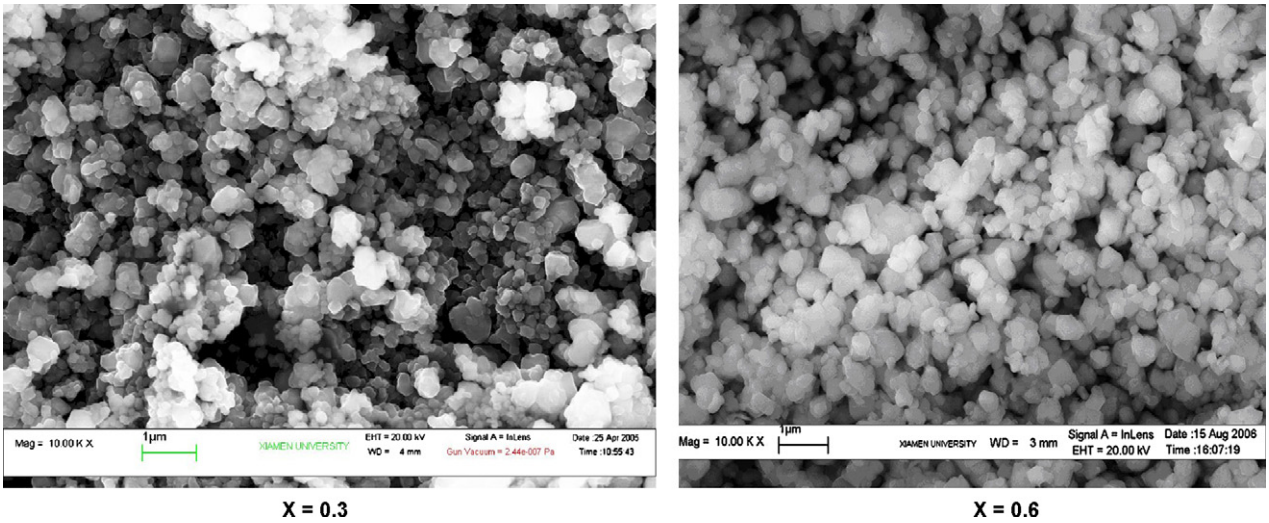

Fig. 5. Scanning electron micrographs of $xLi[Li_{1/3}Mn_{2/3}]O_2\cdot(1-x)Li[Ni_{1/3}Mn_{1/3}Co_{1/3}]O_2$ materials.

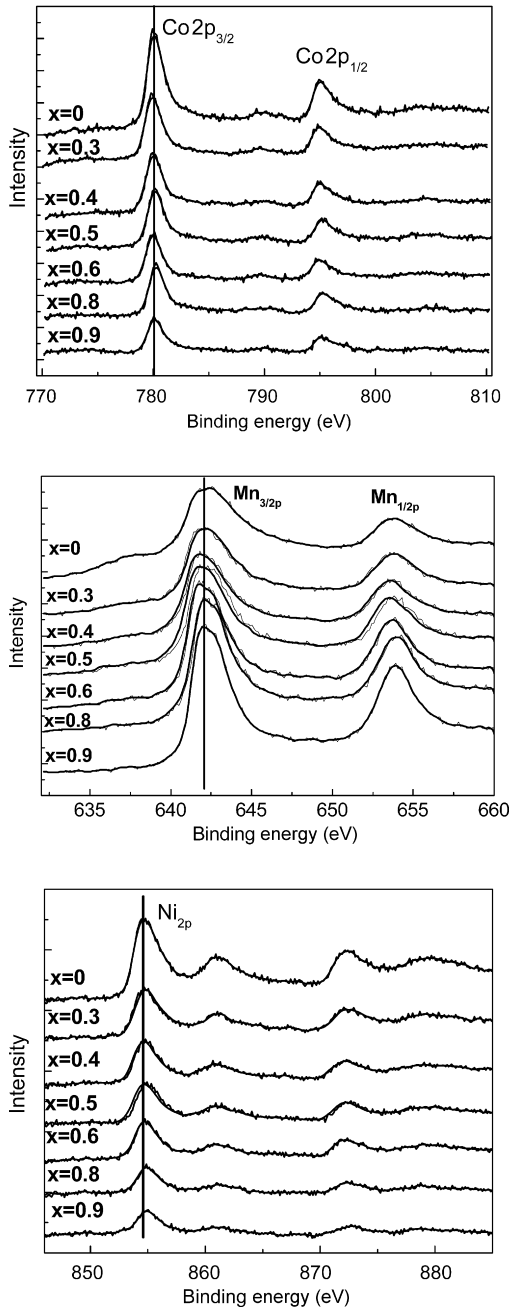

Fig. 6. XPS spectra of Mn 2p, Ni 2p and Co 2p in $x\mathrm{Li[Li_{1/3}Mn_{2/3}]O_2}\cdot(1-x)\mathrm{Li[Ni_{1/3}Mn_{1/3}Co_{1/3}]O_2}$ ($0 \le x \le 0.9$).

cobalt ions in the materials with x. And the redox peaks at 2.5 V in discharging and at near 3.0 V in charging may be attributed to the reduction of Mn^{4+} to Mn^{3+} and the oxidation of Mn^{3+} to Mn^{4+}, which results from the Mn-rich phase in the presence of higher x. It may also be attributed to Mn^{3+}/Mn^{4+} redox couple arising from Li insertion to tetrahedral and octahedral site in the materials which is partially transformed to spinel structures in discharging reactions.

Fig. 9 shows the cycling performances of the $x\mathrm{Li[Li_{1/3}Mn_{2/3}]O_2}\cdot(1-x)\mathrm{Li[Ni_{1/3}Mn_{1/3}Co_{1/3}]O_2}$ electrode materials with $x = 0.3$, 0.5, 0.6, and 0.8 when cycled between 2.0 and 4.8 V at 18 mA g^{-1}. It shows that all the samples show good cycling performance. And, the sample $0.6\mathrm{Li[Li_{1/3}Mn_{2/3}]O_2}\cdot0.4\mathrm{Li[Ni_{1/3}Mn_{1/3}Co_{1/3}]O_2}$ ($x = 0.6$) shows the highest discharge capacity. The good cycling performance of these materials can be attributed to the $\mathrm{Li[Li_{1/3}Mn_{2/3}]O_2}$ component can provide additional stability to the layered $\mathrm{Li[Ni_{1/3}Mn_{1/3}Co_{1/3}]O_2}$ electrode over a wide operating voltage window (such as 2.0–4.8 V) [11]. Based on all of the results shown above, it is believed that $0.6\mathrm{Li[Li_{1/3}Mn_{2/3}]O_2}\cdot0.4\mathrm{Li[Ni_{1/3}Mn_{1/3}Co_{1/3}]O_2}$ ($x = 0.6$) could be developed as a high capacity cathode material for Li ion batteries. The exceptionally high specific capacity and good cyclic performance of the $0.6\mathrm{Li[Li_{1/3}Mn_{2/3}]O_2}\cdot0.4\mathrm{Li[Ni_{1/3}Mn_{1/3}Co_{1/3}]O_2}$ electrode indicate that the $\mathrm{Li[Li_{1/3}Mn_{2/3}]O_2}$ component can stabilize the layered component $\mathrm{Li[Ni_{1/3}Mn_{1/3}Co_{1/3}]O_2}$ at high potentials. Decreasing the $\mathrm{Li[Li_{1/3}Mn_{2/3}]O_2}$ content (x) will result in lower stability of the $x\mathrm{Li[Li_{1/3}Mn_{2/3}]O_2}\cdot(1-x)\mathrm{Li[Ni_{1/3}Mn_{1/3}Co_{1/3}]O_2}$ electrode at high delithiated state, thus lower capacity of the materials. At higher $\mathrm{Li[Li_{1/3}Mn_{2/3}]O_2}$ content (x), the discharge–charge capacity of $x\mathrm{Li[Li_{1/3}Mn_{2/3}]O_2}\cdot(1-x)\mathrm{Li[Ni_{1/3}Mn_{1/3}Co_{1/3}]O_2}$ decrease with x possibly due to the poorer electronic conductivity caused by the higher Mn^{4+} content and the decrease of the theoretical capacity of $x\mathrm{Li[Li_{1/3}Mn_{2/3}]O_2}\cdot(1-x)\mathrm{Li[Ni_{1/3}Mn_{1/3}Co_{1/3}]O_2}$ with x.

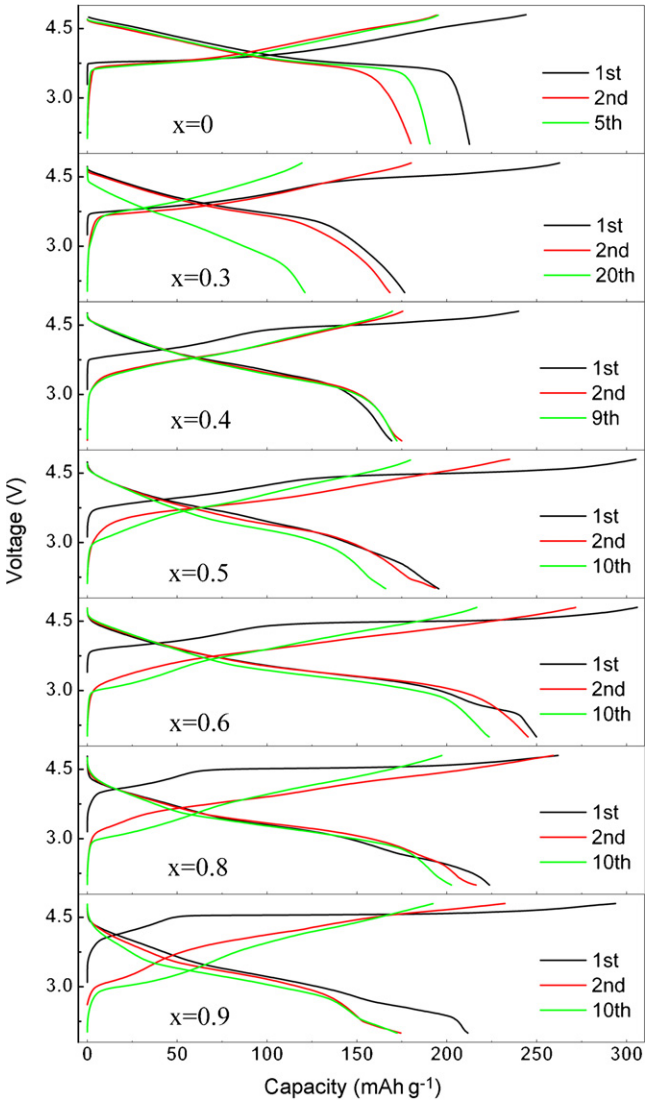

Fig. 7. Voltage profiles vs. capacity of the $\mathrm{Li}/x\mathrm{Li[Li_{1/3}Mn_{2/3}]O_2}\cdot(1-x)\mathrm{Li[Ni_{1/3}Mn_{1/3}Co_{1/3}]O_2}$ ($0 \le x \le 0.9$) cells.

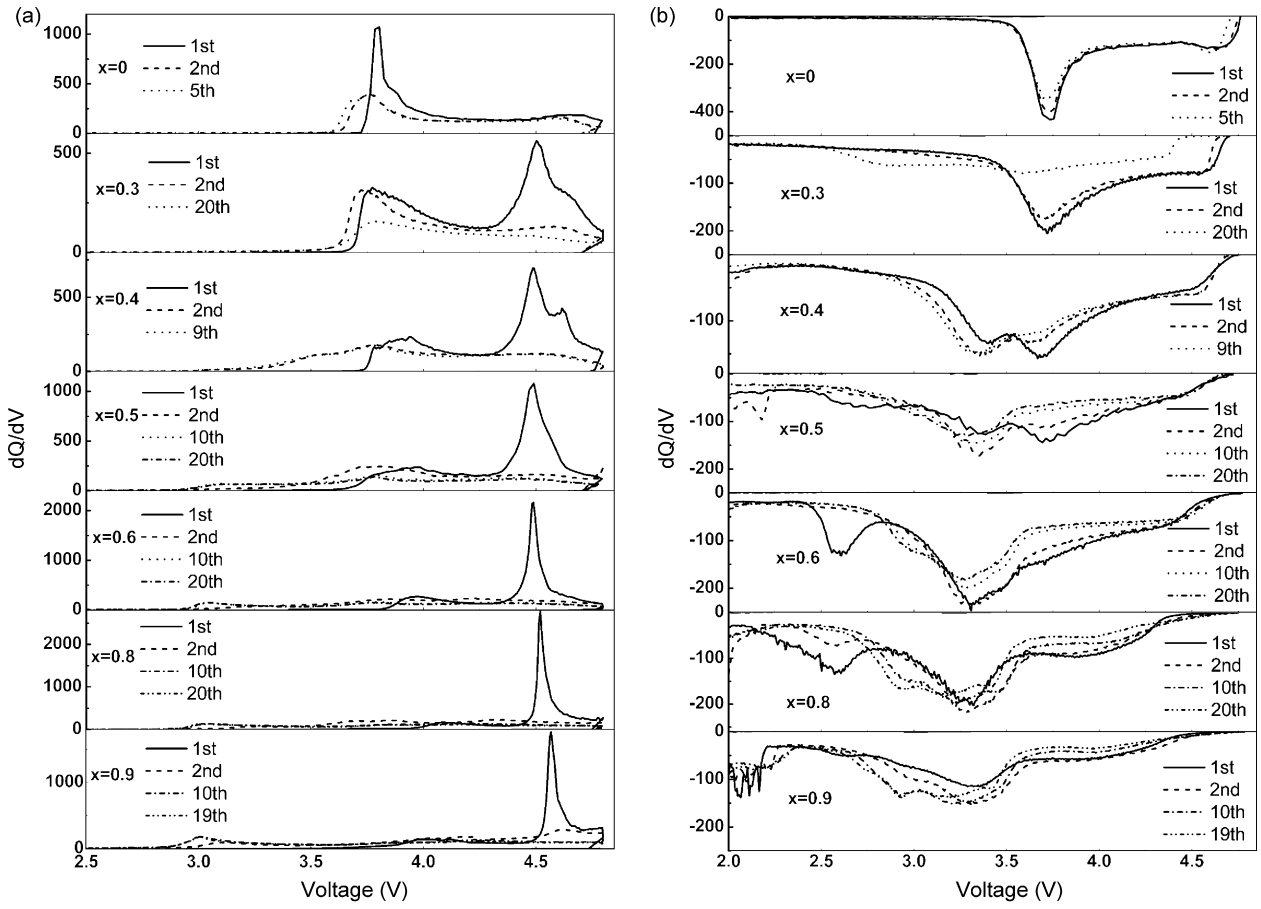

Fig. 8. The differential capacity vs. voltage of the Li/xLi[$Li_{1/3}Mn_{2/3}$]O_2·$(1-x)$Li[$Ni_{1/3}Mn_{1/3}Co_{1/3}$]O_2 ($0 \le x \le 0.9$) cells (a is charging part, b is discharging part).

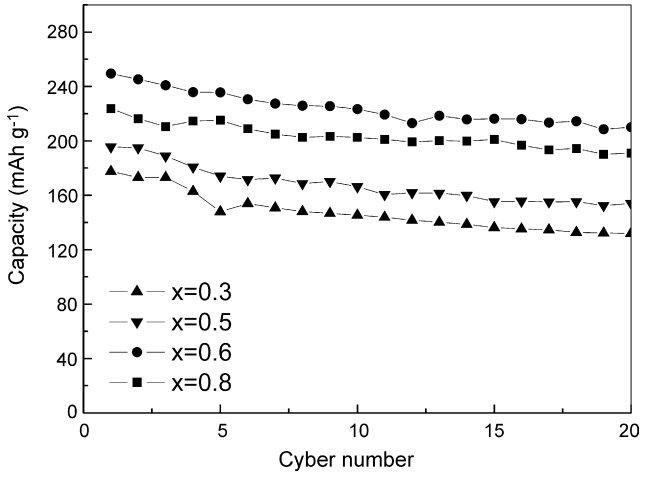

Fig. 9. Cyclic performances of the Li/xLi[$Li_{1/3}Mn_{2/3}$]O_2·$(1-x)$Li[$Ni_{1/3}Mn_{1/3}Co_{1/3}$]O_2 ($0 \le x \le 0.9$) cells.

4. Conclusions

xLi[$Li_{1/3}Mn_{2/3}$]O_2·$(1-x)$Li[$Ni_{1/3}Mn_{1/3}Co_{1/3}$]O_2 ($0 \le x \le 0.9$) were synthesized successfully by combination of co-precipitation and solid state calcination method. The resulting compounds showed good performance in terms of initial capacity and cycle life. The valence state of Mn, Ni, Co is +4, +2, +3, respectively. For 0.6Li[$Li_{1/3}Mn_{2/3}$]O_2·0.4Li[$Ni_{1/3}Mn_{1/3}Co_{1/3}$]O_2 ($x = 0.6$) sample, a high capacity of 250 mAh g^{-1} with good cyclic performance has been achieved.

Acknowledgements

This work was financially supported by National Basic Research Program of China (973 Program) (Grant No. 2007CB209702), and National Natural Science Foundation of China (NNSFC, Grant Nos. 29925310, 20433060).

References

[1] M.S. Whittingham, Chem. Rev. 104 (2004) 4271.
[2] T. Ohzuku, Y. Makimura, Chem. Lett. 30 (2001) 744.
[3] K.M. Shaju, G.V.S. Rao, B.V.R. Chowdari, Electrochim. Acta 48 (2002) 145.
[4] J. Li, Z.R. Zhang, X.J. Guo, Y. Yang, Solid State Ionics 177 (2006) 1509.
[5] J. Li, J.M. Zheng, X.J. Guo, Z.L. Gong, Y. Yang, Chem. J. Chin. Univ. 27 (2006) 1311.
[6] J. Li, J.M. Zheng, Y. Yang, J. Electrochem. Soc. 154 (2007) A427.
[7] N. Yabuuchi, T. Ohzuku, J. Power Sources 119–121 (2003) 171.
[8] C.M. Julien, M. Massot, Mater. Sci. Eng. B 100 (2003) 69.
[9] Z.H. Lu, D.D. MacNeil, J.R. Dahn, Electrochem. Solid State Lett. 4 (2001) A191.
[10] Z.H. Lu, L.Y. Beaulieu, R.A. Donaberger, C.L. Thomas, J.R. Dahn, J. Electrochem. Soc. 149 (2002) A778.
[11] M.M. Thackeray, S.-H. Kang, C.S. Johnson, J.T. Vaughey, R. Benedeka, S.A. Hackney, J. Mater. Chem. 17 (2007) 3112.
[12] J.H. Kim, C.W. Park, Y.K. Sun, Solid State Ionics 164 (2003) 43.
[13] D. Alastair, G. Roberston, P. Bruce, Chem. Mater. 15 (2003) 1984.
[14] J.S. Kim, C.S. Johnson, J.T. Vaughey, M.M. Thackeray, Chem. Mater. 16 (2004) 196.

[15] Z.H. Lu, J.R. Dahn, J. Electrochem. Soc. 149 (2002) A815.
[16] Z.L. Gong, H.S. Liu, X.J. Guo, Z.R. Zhang, Y. Yang, J. Power Sources 136 (2004) 139.
[17] Y.S. Meng, G. Ceder, C.P. Grey, W.-S. Yoon, M. Jiang, J. Bréger, Y. Shao-Horn, Chem. Mater. 17 (2005) 2386.
[18] A.R. Armstrong, M. Holzapfel, P. Novák, C.S. Johnson, S.-H. Kang, M.M. Thackeray, P.G. Bruce, J. Am. Chem. Soc. 128 (2006) 8694–8698.
[19] W. Li, J.N. Reimers, J.R. Dahn, Solid State Ionics 67 (2003) 120.
[20] H.S. Liu, J. Li, Z.R. Zhang, Z.L. Gong, Y. Yang, Electrochim. Acta 49 (2004) 1151.
[21] B.E. Warren, X-ray Diffraction, Dover Publications, New York, 1990.